Superconductivity in pressurized CeRhGe_{3} and related noncentrosymmetric compounds

Honghong Wang, Jing Guo, Eric D. Bauer, Vladimir A. Sidorov, Hengcan Zhao, Jiahao Zhang, Yazhou Zhou, Zhe Wang, Shu Cai, Ke Yang, Aiguo Li, Xiaodong Li, Yanchun Li, Peijie Sun, Yi-feng Yang, Qi Wu, Tao Xiang, J. D. Thompson, and Liling Sun

Phys. Rev. B **97**, 064514 — Published 20 February 2018

DOI: 10.1103/PhysRevB.97.064514

Superconductivity in pressurized $CeRhGe_3$ and related non-centrosymmetric compounds

Honghong Wang[1,6]*, Jing Guo[1]*, Eric D. Bauer[2],Vladimir A. Sidorov[3], Hengcan Zhao[1,6], Jiahao Zhang[1,6], Yazhou Zhou[1], Zhe Wang[1,6],Shu Cai[1,6], Ke Yang[4],Aiguo Li[4], Xiaodong Li[5], Yanchun Li[5], Peijie Sun[1], Yi-feng Yang[1,6], Qi Wu[1], Tao Xiang[1,6], J. D. Thompson[2]†,Liling Sun[1,6]†

[1]*Institute of Physics, National Laboratory for Condensed Matter Physics, Chinese Academy of Sciences, Beijing 100190, China*

[2]*Los Alamos National Laboratory, MS K764, Los Alamos, NM 87545, USA*

[3]*Institute for High Pressure Physics, Russian Academy of Sciences, 142190 Troitsk, Moscow, Russia*

[4]*Shanghai Synchrotron Radiation Facilities, Shanghai Institute of Applied Physics, Chinese Academy of Sciences, Shanghai 201204, China*

[5]*Institute of High Energy Physics, Chinese Academy of Science, Beijing 100049, China*

[6]*University of Chinese Academy of Sciences, Beijing 100190, China*

We report the discovery of superconductivity in pressurized $CeRhGe_3$, until now the only remaining non-superconducting member of the isostructural family of non-centrosymmetric heavy-fermion compounds $CeTX_3$ (T = Co, Rh, Ir and X = Si, Ge). Superconductivity appears in $CeRhGe_3$ at a pressure of 19.6 GPa and the transition temperature T_C reaches a maximum value of 1.3 K at 21.5 GPa. This finding provides an opportunity to establish systematic correlations between superconductivity and material properties within this family. Though ambient-pressure unit-cell volumes and critical pressures for superconductivity vary substantially across the series, all family members reach a maximum T_C^{max} at a common (±1.7%) critical cell volume V_{crit}, and T_C^{max} at V_{crit} increases with increasing spin-orbit coupling strength of the *d*-electrons. These correlations show that substantial Kondo and spin-orbit couplings favor superconductivity in this family, the latter reflecting the role of broken centrosymmetry.

PACS numbers: 74.70.Tx, 71.27.+a, 74.62.Fj

I. INTRODUCTION

The discovery of the first heavy-fermion superconductor $CeCu_2Si_2$ in 1979 [1] opened the new field of unconventional superconductivity and posed a fundamental challenge for understanding the superconducting mechanism. After nearly forty years, more than forty heavy-fermion superconductors have been found, and there is growing appreciation that their superconductivity emerges at the border of competing or coexisting electronic orders [2], suggesting that fluctuations of these orders may be the source of superconductivity. Among heavy-fermion compounds, the $CeTX_3$ (T = Co, Ir, Rh and X = Si, Ge) [3,4] family belongs to a subset whose crystallographic structure (*I*4*mm*) lacks a center of inversion symmetry [5,6]. Except for the mixed-valence member $CeCoSi_3$, others of the family order antiferromagnetically at atmospheric pressure. Application of pressure to $CeRhSi_3$, $CeIrSi_3$ and $CeCoGe_3$ $CeIrGe_3$ suppresses their Néel temperature toward zero temperature where a dome of superconductivity emerges [7-18]. These observations have led to suggestions that magnetic fluctuations may induce unconventional superconductivity, but this remains unsettled, in part because of the possible non-trivial role of antisymmetric spin-orbit coupling that is a consequence of these materials' non-centrosymmetry [6]. Beside its possible role in forming superconductivity, sufficiently strong spin-orbit coupling would also lead to an unusual pairing state that is a mixture of spin-singlet and spin-triplet components.

As a member of the magnetic $CeTX_3$ family, $CeRhGe_3$ is expected to become superconducting under pressure. However, experiments to about 8 GPa find only a

monotonic increase in its Néel temperature [15]. Here, we report the first observation of pressure-induced superconductivity in $CeRhGe_3$. As will be discussed, this discovery allows a broader perspective on conditions favoring superconductivity in this family of nominally isoelectronic compounds.

II. EXPRIMENTAL DETAILS

Single crystals of $CeRhGe_3$ were grown from a $Rh_{0.25}Ge_{0.75}$ eutectic self-flux (T_{melt} = 850 ℃) [19,20]. The elements Ce, Rh, Ge were arc-melted together in a molar ratio of Ce:Rh:Ge = 1:3.5:13.5 (corresponding to $CeRhGe_6$ + 10 $Rh_{0.25}Ge_{0.75}$) on a water-cooled copper hearth in an ultra-high purity Ar atmosphere. The arc-melted button was then placed in a 2-ml alumina crucible and sealed under vacuum in a silica tube. The tube was heated to 1150 ℃, held at that temperature for 12 hours, and then cooled slowly at 2 ℃/hr to 875 ℃. The excess flux was removed by spinning the (inverted) silica tube in a centrifuge. Single crystals of $CeRhGe_3$ in the form of three-dimensional, tetrahedral-like blocks with well-defined facets and volumes ranging from 1-4 mm^3 were obtained.

High-pressure resistance and magnetoresistance measurements were carried out in a diamond-anvil cell made of a Be-Cu alloy. Diamond anvils with 300-μm flats were used for all high-pressure experiments. In the resistance measurements, NaCl powder was employed as the pressure-transmitting medium to obtain a quasi-hydrostatic pressure environment, which has been widely used for high pressure transport measurements [21]. Four-probe method determined the *ab* plane resistance

of the single-crystal sample. In our high-pressure *ac* susceptibility measurements, the sample is surrounded by a the secondary coil (pickup coil) and a field generating primary coil wound on top of the secondary coil. The alternating flux through the pickup coil produces an *ac* voltage which is the measured signal. When the sample is cooled below T_C, the field is expelled from the sample due to the superconducting shielding effect, forcing some of the flux lines out of the pickup coil and leading to a reduction in the induced voltage in the pickup coil [22-25]. A Lock-in amplifier (SR830) is used to generate *ac* magnetic field through the primary coil and to detect the drop in the induced voltage through the secondary coil. The frequency used for the χ' data is 217 Hz, and the primary coil yields a magnetic field of 3 Oe at this frequency. The balanced secondary coils are connected with a lock-in amplifier. In order to minimize this temperature-dependent background, we used high pressure cell made from Be-Cu alloy to generate pressure and Be-Cu sheet as a gasket because Be-Cu alloy is non-magnetic material. Even so, we first measured the *ac* susceptibility for the high pressure cell without sample but with coils and gaskets to get the background, and then performed the *ac* susceptibility measurement for the sample in the same high pressure cell. To pick up the signal from the sample carefully, we did the background subtraction.

High-pressure X-ray diffraction (XRD) measurements were performed at room temperature on beamline 15U at the Shanghai Synchrotron Radiation Facility and beamline 4W2 at the Beijing Synchrotron Radiation Facility. Diamonds with low birefringence were selected for these XRD measurements. A monochromatic X-ray

beam with a wavelength of 0.6199 Å was employed and silicon oil served as a pressure-transmitting medium [26-28].

The high-pressure heat capacity of the sample under pressure was derived from *ac* calorimetry. Pressure is determined by the pressure dependence of T_C of Pb [29] that is placed together with the sample in a Teflon capsule. In this technique, a small temperature oscillation ΔT generated by a heater glued to one face of the crystal is converted to an *ac* voltage signal by a chromel-AuFe (0.07%) thermocouple fixed on the opposite side and $C \propto 1/T$. The pressure for all measurements in a diamond-anvil cell was determined by the ruby fluorescence method [30].

III. RUSULTS AND DISCUSSIONS

High-pressure heat capacity measurements down to 4 K reveal two anomalies that, like $CeIrGe_3$ [4], are associated with AFM transitions (see Fig. 1). We denote the higher AFM transition as T_{N1} and the lower one by $T_{N2.}$ These two AFM transitions at T_{N1} and T_{N2} are identified from our high pressure resistance measurements and the minima in second derivatives of the resistivity (Fig.2 and Fig.3). Figure 2a shows temperature dependence of resistance for $CeRhGe_3$ at ambient pressure, from which T_{N1} and T_{N2} can be observed (as indicated by arrows in the inset of the figure). With increasing pressure, T_{N1} and T_{N2} move to higher temperatures (Fig.2b and Fig.3a), consistent with the previously reported pressure dependence of T_{N1} [15]. T_{N1} reaches a maximum at 8.5 GPa and T_{N2} is maximized near 10.5 GPa. Both transitions decrease at higher pressures and merge at ~13.7 GPa

within experimental resolution. This is seen most clearly in the pressure evolution of $\partial^2 R/\partial T^2$ shown in Fig.3a. The merged AFM transition temperature T_N falls monotonically with increasing pressure up to 18.6 GPa (Fig.2c and Fig.3b). This merging of two antiferromagnetic transitions and its pressure dependence are similar to that reported for $CeIrGe_3$ [12]. At 20.5 GPa, we found a resistive drop at ~ 1 K (inset of Fig.2c). To investigate the new resistive trop, we carried out a new experimental run (Fig.2d). It is see that, at 19.6 GPa where T_N = 3.6 K (as indicated by the arrow in the inset of Fig.2d), there is a pronounced drop in resistance at ~1.1 K. This resistance drop is largest at 21.5 GPa, where the resistance declines by ~76.6 %, and then the drop becomes smaller upon further compression (Fig.2d). This observation is confirmed in a separate measurement in which a pressure-induced resistance drop is ~92.8 % at 22.0 GPa, as shown in Fig. 2f. To explore the origin of this resistance drop, we applied a magnetic field to $CeRhGe_3$ subjected to 21.5 GPa and cooled the high-pressure cell to 40 mK. As shown in Fig.2e the onset temperature of the resistance drop shifts to lower temperature upon increasing magnetic field. Furthermore, *ac* susceptibility measured at 20.1 GPa (the inset of Fig.2e) becomes diamagnetic at ~1.2 K. All these measurements show that the pressure-induced resistance drop in low temperatures results from a superconducting transition.

To know the superconducting volume in our sample, we used the same high pressure cell and the gasket to perform the susceptibility measurement on lead (Pb) which is considered to have 100% superconducting volume. It is found that the

voltage drop from Pb in the pickup coil is about 28 nV. Consequently, we can estimate the superconducting volume of our sample that is subjected to 20.1 GPa and its superconductivity coexists with AFM order to be about 11%. Based on these results, we propose that the superconductivity at 20.1 GPa is likely a filamentary-like superconductivity, in good agreement with a body of evidence in correlated electron materials that filamentary-like superconductivity develops above the bulk superconducting transition when antiferromagnetic order is present and that the resistive T_C nearly coincides with the bulk T_C once evidence for magnetic order is absent [31,32]. Note that the resistance below the onset temperature is still finite which is possibly due to the presence of sample micro-cracks generated by the quasi-hydrostatic pressure environment.

We extract the field dependence of T_C for $CeRhGe_3$ at 21.5 GPa (Fig. 2e) and display it in Fig.4. We did a linear-fit for the magnetic dependence of T_C (as shown by dashed line in Fig.4). The rate of decrease of the onset temperature is very high (-11.6 T/K), a huge value that a characteristic of the weak temperature dependence of the magnetic field of pressure-induced superconductivity in other $CeTX_3$ compounds [5]. Extrapolation of the linear-fit to zero temperature yields upper critical pressure about 15 T at 21.5 GPa.

This pressure-induced superconductivity emerges in the non-centrosymmetric *I*4*mm* crystal structure. Results of synchrotron X-ray diffraction (XRD) measurements on $CeRhGe_3$ at pressures up to 28.5 GPa are summarized in Fig. 5. With increasing pressure, the lattice constants decrease, but the crystal structure remains unchanged. A

fit of the pressure-dependent cell volume to a Murnaghan equation of state ($V = V_0 \times [1 + P \times (B'/B)]^{-1/B'}$) gives a bulk modulus ($B$) and its pressure derivative (B') of 115 GPa and 5, respectively. Here B is the isothermal bulk modulus at zero pressure, B' is the pressure derivative of B evaluated at zero pressure, and V and V_0 are the high-pressure volume and zero-pressure volume of the material, respectively. The stability of the structure against pressure rules out the possibility that the superconductivity emerges in a different crystal structure at low temperatures. This is consistent with the observation of the huge $\partial H_{C2}/\partial T$ of $CeRhGe_3$ which is a common feature of these non-centrosymmetric superconductors.

Figure 6 shows the pressure-temperature phase diagram obtained from our measurements. The overall bell-shaped response of antiferromagnetism to applied pressure is captured in Doniach's model of competing Ruderman-Kittel-Kasuya-Yosida (RKKY) and Kondo interactions [33]. With increasing pressure, the Kondo hybridization becomes dominant, which suppresses the RKKY-mediated long-range order. However, T_N does not go continuously to zero temperature. A similar pressure dependence of the AFM transition temperature is also found in $CeIrGe_3$ [12]. Nevertheless, the substantially suppressed Néel order around 20 GPa leaves the possibility that magnetic fluctuations could play a role in inducing superconductivity that initially coexists with antiferromagnetic order.

In Fig. 7a we place our discovery of superconductivity in $CeRhGe_3$ in the context of early results on other members of the $CeTX_3$ family [4-13,15,18] and compare the pressure dependence of the superconducting transition temperature for the whole

$CeTX_3$ family. We find that the critical pressure P_{crit} at which pressure-induced superconductivity reaches a maximum T_C is strongly correlated with the unit-cell volume at the ambient pressure (Fig.7a). For X = Si or Ge, the cell volume increases in the sequence T = Co, Rh, Ir, and for a given T, the cell volume is larger for X = Ge. $CeCoSi_3$, with the smallest cell volume, has a mixed-valence 4*f*-configuration reflecting strong hybridization between *f* and conduction (*c*) electrons and is not superconducting above 0.5 K [34]. In contrast, the Kondo hybridization in the large-cell compounds, $CeIrGe_3$ and $CeRhGe_3$, is much weaker [4]. As the unit cell expands, the critical pressure P_{crit} increases by an order of magnitude from $CeRhSi_3$ to $CeIrGe_3$. This correlation implies that an optimally large hybridization and, thus, an optimally strong Kondo coupling induced by compression are required for superconductivity.

Assuming that our equation of state for $CeRhGe_3$ provides a reasonable approximation for estimating the cell volume of other $CeTX_3$ members at P_{crit}, we plot in Fig. 7b the maximum superconducting transition temperature T_C^{max} as a function of critical cell volume V_{crit} at P_{crit}. Interestingly, all T_C^{max} fall within a rather narrow range of V_{crit} values that vary by only ±1.7%, as emphasized by the vertical dashed lines in Fig. 7a. It appears, then, that there is an approximate optimal cell volume for achieving a maximum T_C. Because all the family members are nominally isoelectronic, this correlation could be interpreted as reflecting an optimal hybridization/Kondo coupling for a maximum T_C. Further, as shown by dashed lines in Fig. 7a, V_{crit}, and by inference a critical hybridization/Kondo coupling strength,

places optimal superconductivity near the cross-over to a mixed-valence regime found in $CeCoSi_3$. This raises the possibility that critical valence fluctuations also might play a role in producing superconductivity in the $CeTX_3$ series, with $CeCoSi_3$ being too far into the mixed-valence regime for those fluctuations to be effective.

Perhaps the most interesting correlation is that T_C^{max} increases systematically as the T element changes from 3*d* to 4*d* to 5*d*, and for T = Rh and Ir, T_C^{max} is similar irrespective of the X element. With a fixed angular momentum of the T elements, the atomic spin-orbit interaction strength, which gives rise to a Rashba antisymmetric spin-orbit coupling [6], is proportional to Z^4/n^3, where Z is the atomic number and n is the principal quantum number. Normalizing this ratio to 1 for T = Co, then the atomic spin-orbit coupling is ~3 and ~14 times stronger for T = Rh and Ir, respectively. The observation that T_C^{max} is comparable for T = Rh and Ir irrespective of X suggests that spin-orbit coupling of the X elements may not play such an important role, and, indeed, X elements tend to act as 'inert' spacers. As an aside, we note that of all the members, $CeCoGe_3$ is the only one with a magnetic easy-plane, as opposed to others with an easy-axis [7], and $CeCoSi_3$ is strongly hybridized. The clear correlation in Fig. 7b is that T_C^{max} increases with increasing spin-orbit coupling strength.

The role of antisymmetric spin-orbit coupling is to lift spin degeneracy of single-particle states, removing parity symmetry and creating spin-split electronic bands in which spins are polarized tangential to the electrons' momentum. In general, band splitting due to antisymmetric spin-orbit coupling is band-dependent, and an effective antisymmetric spin-orbit coupling is expected to depend on the extent of

hybridization between *f* and conduction electrons [35]. Though a correlation between T_C^{max} and magnitude of the atomic spin-orbit coupling is obvious in Fig. 7b, the correlation is not 1:1 because *f-c* hybridization, and hence effective antisymmetric spin-orbit coupling, varies with the T element. From results in Fig. 7, we conclude, then, that spin-orbit coupling is a key factor in determining the maximum value of T_C in the $CeTX_3$ family and that a narrow range of cell volumes, *i.e.*, hybridization, is necessary for inducing a superconducting state.

IV. CONCLUSION

We have discovered superconductivity in heavy-fermion $CeRhGe_3$, the last non-superconducting member of the $CeTX_3$ family. This discovery has allowed a new perspective on conditions necessary for superconductivity in the family and for the maximum T_C that its members reach. It is not possible from our studies to make definitive statements about the pairing mechanism or symmetry of the superconducting pairs, but it seems that magnetic as well as valence fluctuations could be effective in Cooper pairing and that, with higher maximum T_C's in the sequence X = 3*d*, 4*d* to 5*d*, spin-orbit coupling plays a progressively dominant role in determining the gap symmetry. Clearly, this work calls for new experiments to determine the evolution of the relative admixture of spin-singlet and spin-triplet pairing across the series, to search for evidence of valence and magnetic fluctuations in the vicinity of V_{crit}, and for theory that explicitly considers antisymmetric spin-orbit coupling, not only for its effect on the pairing symmetry but also as an initial

condition for superconductivity in $CeTX_3$ materials and in non-centrosymmetric compounds more broadly.

References

[1] F. Steglich, J. Aarts, C. D. Bredl, W. Lieke, D. Meschede, W. Franz, and H. Schäfer, Phys. Rev. Lett. **43**, 1892 (1979).

[2] C. Pfleiderer, Rev. Mod. Phys. **81**, 1551 (2009).

[3] P. Haen, P. Lejay, B. Chevalier, B. Lloret, J. Etourneau, and M. Sera, Journal of the Less Common Metals **110**, 321 (1985).

[4] Y. Muro, D. Eom, N. Takeda, and M. Ishikawa, J. Phys. Soc. Jpn. **67**, 3601 (1998).

[5] N. Kimura and I. Bonalde, in *Non-Centrosymmetric Superconductors*, edited by E. Bauer and M. Sigrist (Springer,Berlin, 2012), pp. 35-79.

[6] M. Smidman, M. B. Salamon, H. Q. Yuan, and D. F. Agterberg, Rep. Prog. Phys. **80**, 036501 (2017).

[7] T. Kawai, H. Muranaka, M.-A. Measson, T. Shimoda, Y. Doi, T. D. Matsuda, Y. Haga, G. Knebel, G. Lapertot, D. Aoki, J. Flouquet, T. Takeuchi, R. Settai, and Y. Ōnuki, J. Phys. Soc. Jpn. **77**, 064716 (2008).

[8] I. Sugitani, Y. Okuda, H. Shishido, T. Yamada, A. Thamizhavel, E. Yamamoto, T. D. Matsuda, Y. Haga, T. Takeuchi, R. Settai, and Y. Ōnuki, J. Phys. Soc. Jpn. **75**, 043703 (2006).

[9] N. Kimura, K. Ito, K. Saitoh, Y. Umeda, H. Aoki, and T. Terashima, Phys. Rev.

Lett. **95**, 247004 (2005).

[10] R. Settai, Y. Okuda, I. Sugitani, Y. Ōnuki, T. D. Matsuda, Y. Haga, and H. Harima, Int. J. Mod. Phys. B **21**, 3238 (2007).

[11] G. Knebel, D. Aoki, G. Lapertot, B. Salce, J. Flouquet, T. Kawai, H. Muranaka, R. Settai, and Y. Ōnuki, J. Phys. Soc. Jpn. **78**, 074714 (2009).

[12] F. Honda, I. Bonalde, K. Shimizu, S. Yoshiuchi, Y. Hirose, T. Nakamura, R. Settai, and Y. Ōnuki, Phys. Rev. B **81**, 140507(R) (2010).

[13] N. Kimura, K. Ito, H. Aoki, S. Uji, and T. Terashima, Phys. Rev. Lett. **98**, 197001 (2007).

[14] R. Settai, Y. Miyauchi, T. Takeuchi, F. Lévy, I. Sheikin, and Y. Ōnuki, J. Phys. Soc. Jpn. **77**, 073705 (2008).

[15] T. Kawai, M. Nakashima, Y. Okuda, H. Shishido, T. Shimoda, T. D. Matsuda, Y. Haga, T. Takeuchi, M. Hedo, Y. Uwatoko, R. Settai, and Y. Ōnuki, J. Phys. Soc. Jpn. **76**, 166 (2007).

[16] T. Sugawara, H. Iida, H. Aoki, and N. Kimura, J. Phys. Soc. Jpn. **81**, 054711 (2012).

[17] J. F. Landaeta, D. Subero, D. Catalá, S. V. Taylor, N. Kimura, R. Settai, Y. Ōnuki, M. Sigrist, and I. Bonalde, arXiv preprint arXiv:1702.06812 (2017).

[18] N. Kimura, Y. Muro, and H. Aoki, J. Phys. Soc. Jpn. **76**, 051010 (2007).

[19] N. N. Zhuravlev and G. S. Zhdanov Sov. Phys. Crystallogr. **1**, 158, (1956).[20] ASM Alloy Phase Diagrams Center, 2007; data from Okamoto H., Ge-Rh (Germanium-Rhodium), Binary Alloy Phase Diagrams, II Ed., Ed. T. B.

Massalski, Vol. 2, 1990, p 1989-1991

[21] G. J. Piermarini, S. Block, and J. D. Barnett, J. Appl. Phys. **44**, 5377 (1973).

[22] V. G. Tissen, E. G. Ponyatovskii, M. V. Nefedova, F. Porsch, and W. B. Holzapfel, Phys. Rev. B **53**, 8238 (1996).

[23] J. J. Hamlin, V. G. Tissen, and J. S. Schilling, Phys. Rev. B **73**, 094522 (2006).

[24] M. Debessai, J. J. Hamlin, and J. S. Schilling, Phys. Rev. B **78**, 064519 (2008).

[25] L. L. Sun, X.-J. Chen, J. Guo, P. W. Gao, Q.-Z. Huang, H. D. Wang, M. H. Fang, X. L. Chen, G. F. Chen, Q. Wu, C. Zhang, D. C. Gu, X. L. Dong, L. Wang, K. Yang, A. G. Li, X. Dai, H.-K. Mao, and Z. X. Zhao, Nature (London) **483**, 67 (2012).

[26] D. D. Ragan, D. R. Clarke, and D. Schiferl, Rev. Sci. Instrum. **67**, 494 (1996).

[27] Y. Shen, R. S. Kumar, M. Pravica, and M. F. Nicol, Rev. Sci. Instrum. **75**, 4450 (2004).

[28] N. Tateiwa and Y. Haga, Rev. Sci. Instrum. **80**, 123901 (2009).

[29] A. Eiling and J. S. Schilling, Journal of Physics F: Metal Physics **11**, 623 (1981).

[30] H. K. Mao, J. Xu, and P. M. Bell, J. Geophys. Res **91**, 4673 (1986).

[31] T. Park, H. Lee, I. Martin, X. Lu, V. A. Sidorov, K. Gofryk, F. Ronning, E. D. Bauer, and J. D. Thompson, Phys. Rev. Lett. **108**, 077003 (2012).

[32] T. Park, X. Lu, H.-O. Lee, and J. D. Thompson, Physica C: Superconductivity **481**, 223 (2012).

[33] S. Doniach, Physica B&C **91**, 231 (1977).

[34] T. Shimoda, Y. Okuda, Y. Takeda, Y. Ida, Y. Miyauchi, T. Kawai, T. Fujie, I. Sugitani, A. Thamizhavel, T. D. Matsuda, Y. Hagab, T. Takeuchic, M. Nakashima, R. Settai, and Y. Ōnuki, J. Magn. Magn. Mater **310**, 308 (2007).

[35] H. Iida, Y. Kadota, M. Kogure, T. Sugawara, H. Aoki, and N. Kimura, J. Phys. Soc. Jpn. **80**, 083701 (2011).

Acknowledgements

We thank Prof. Frank Steglich for helpful discussions. The work in China was supported by the National Key Research and Development Program of China (Grant No. 2017YFA0303103, 2017YFA0302900, 2016YFA0300300 and 2015CB921303), the NSF of China (Grants No. 11427805, No. U1532267, No. 11604376, No. 11522435), the Strategic Priority Research Program (B) of the Chinese Academy of Sciences (Grant No. XDB07020300). Work at Los Alamos National Laboratory was performed under the auspices of the U.S. DOE, Office of Basic Energy Sciences, Division of Materials Sciences and Engineering.

† Correspondence and requests for materials should be addressed to L.S (llsun@iphy.ac.cn) and J.T (jdt@lanl.gov).

* These authors contributed equally to this work.

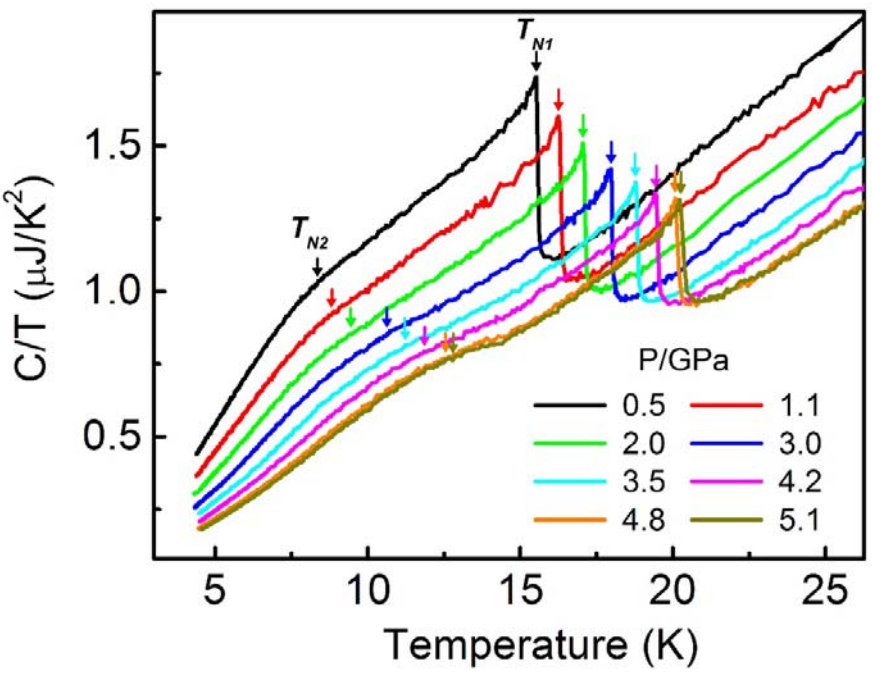

Figure 1 Temperature dependences of heat capacity divided by temperature (*C*/*T*) at different pressures. T_{N1} and T_{N2} correspond to the higher and lower AFM transition temperatures, respectively.

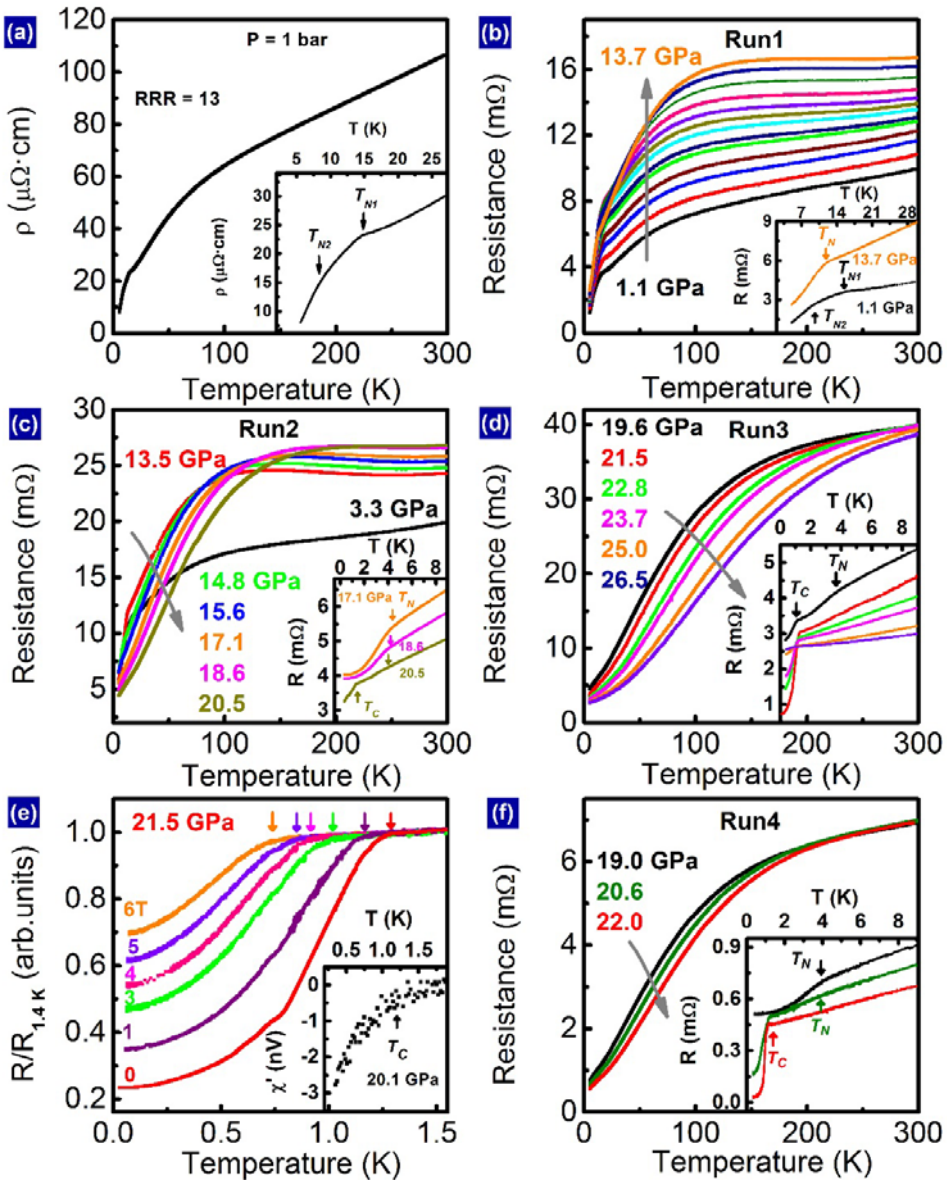

Figure 2 High-pressure electrical resistance and *ac* susceptibility of $CeRhGe_3$. (a) Temperature dependence of resistivity for the ambient-pressure $CeRhGe_3$ sample investigated in this study. RRR of our sample is about 13, similar to the result (RRR = 15) reported by Ref [7]. (b) The temperature dependence of resistance at pressures from 1.1 to 13.7 GPa. The pressures are 1.1, 2.2, 3.4, 4.2, 5.4, 6.3, 7.6, 8.5, 9.3, 10.4, 11.4, 12.7, 13.7 GPa from the bottom to the top. The inset displays evidence for two antiferromagnetic transition temperatures, T_{N1} and T_{N2} (as indicated by arrows), for *P*

= 1.1 GPa that merge together at 13.7 GPa (as indicated by orange arrow). (c) The temperature dependence of resistance for another run in the pressure range of 3.3-20.5 GPa. The inset is an enlarged view of the resistance in the lower temperature regime, showing only one AFM transition at 17.1 GPa and 18.6 GPa, and another resistance drop at low temperatures at 20.5 GPa. (d) The temperature dependence of resistance obtained in the pressure range of 19.6 - 26.5 GPa. The inset is an enlarged view of the resistance in the lower temperature regime. As discussed in the text, the pronounced drop in resistance at low temperatures reflects a pressure-induced superconducting transition. (e) The temperature dependence of the normalized resistance measured at 21.5 GPa under different magnetic fields. The arrows indicate the onset temperature of the superconducting transition. The inset displays the real part of *ac* susceptibility measured at 20.1 GPa. (f) The resistance versus temperature measured in another run where the resistance drop at T_C is more pronounced.

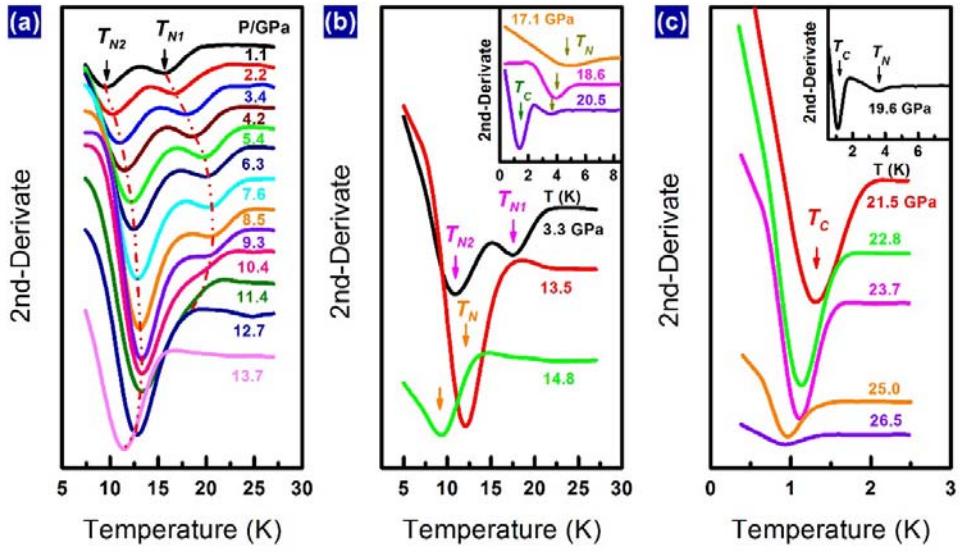

Figure 3 Second derivate of the electrical resistance with respect to temperature for $CeRhGe_3$ crystals at different pressures. (a)-(b) Pressure-induced evolution of transition temperatures T_{N1} and T_{N2} that merge into a single transition T_N. The insets of (b) display details of the second derivate in the lower temperature range near the boundary of antiferromagnetism and superconductivity. (c) Pressure dependence of the superconducting transition temperature T_C as revealed by the second derivative of resistance.

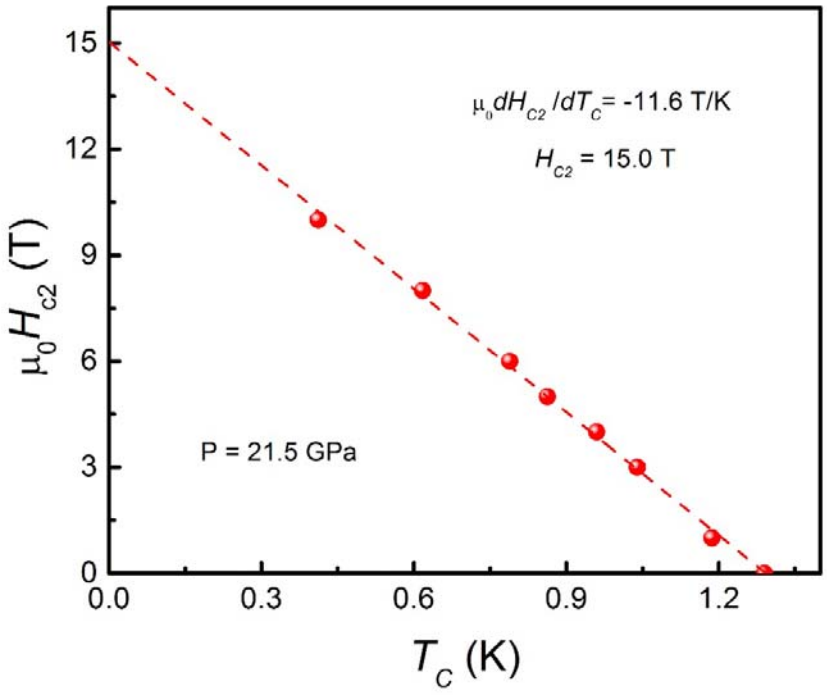

Figure 4 Plot of superconducting transition temperature T_C versus upper critical field for $CeRhGe_3$ at 21.5 GPa. The dashed line represents a linear fit to the data.

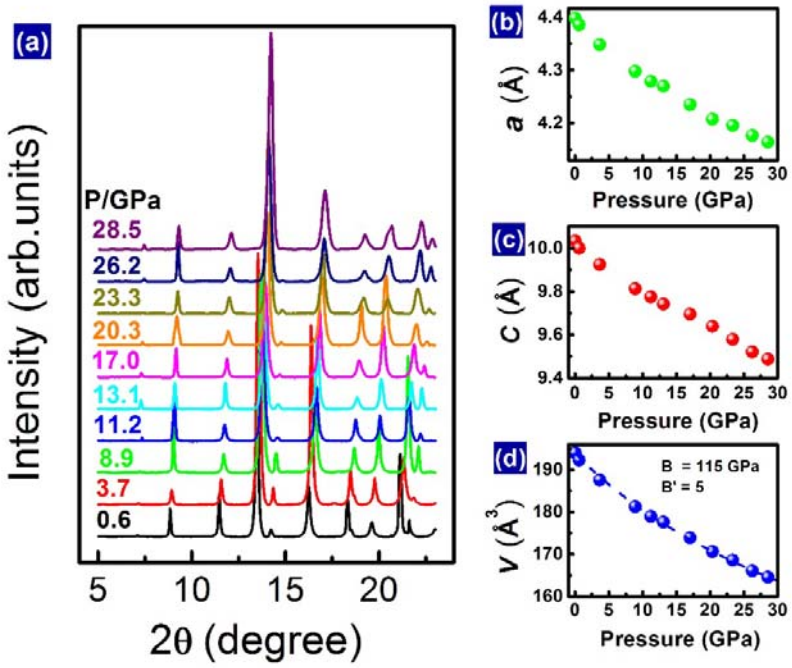

Figure 5 Structure of $CeRhGe_3$ under pressure. (a) X-ray diffraction patterns of $CeRhGe_3$ collected at different pressures, showing no structure phase transition up to 28.5 GPa. (b-d) Pressure dependence of lattice parameters *a, c* and unit cell volume (*V*). The dashed curve in (d) is a fit of data to a Murnaghan equation of state that yields a bulk modulus $B = 115$ GPa and its pressure derivative $B' = 5$.

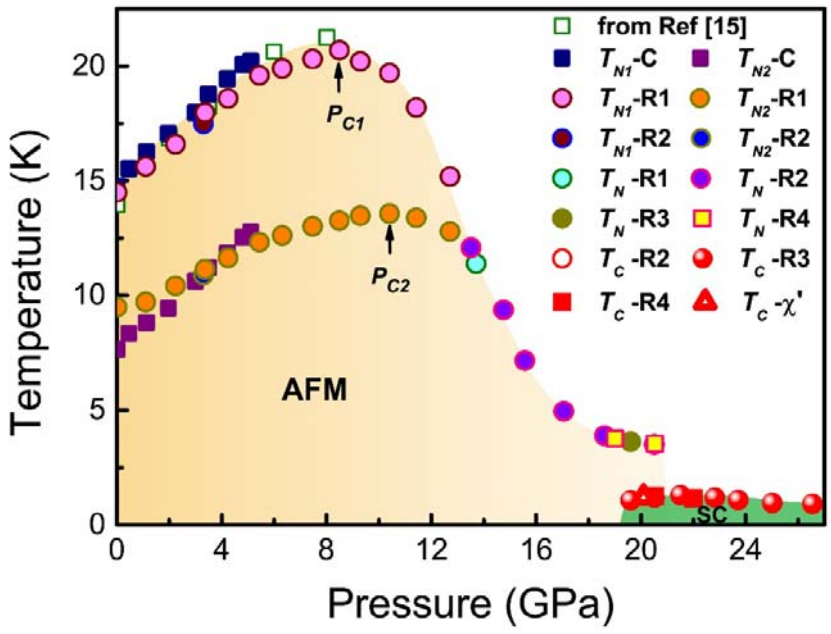

Figure 6 Temperature-pressure phase diagram for $CeRhGe_3$. The solid squares in navy and purple represent the T_{N1} and T_{N2} transition temperatures determined by our high-pressure heat capacity measurements. The solid circles in magenta (wine) and orange (blue) represent the T_{N1} and T_{N2} transition temperatures determined by our high-pressure resistance measurements. P_{C1} and P_{C2} are the critical pressures where the T_{N1} and T_{N2} show a maximum value. The violet (cyan and dark yellow) circles and yellow squares stand for the merged antiferromagnetic transition temperature (T_N) above 13.7 GPa. The solid red circles, squares, open circles and open triangle denote the superconducting transition temperature (T_C) determined by high-pressure resistance and *ac* susceptibility measurements. The olive squares are T_{N1} transition temperatures adopted from Ref. [15].

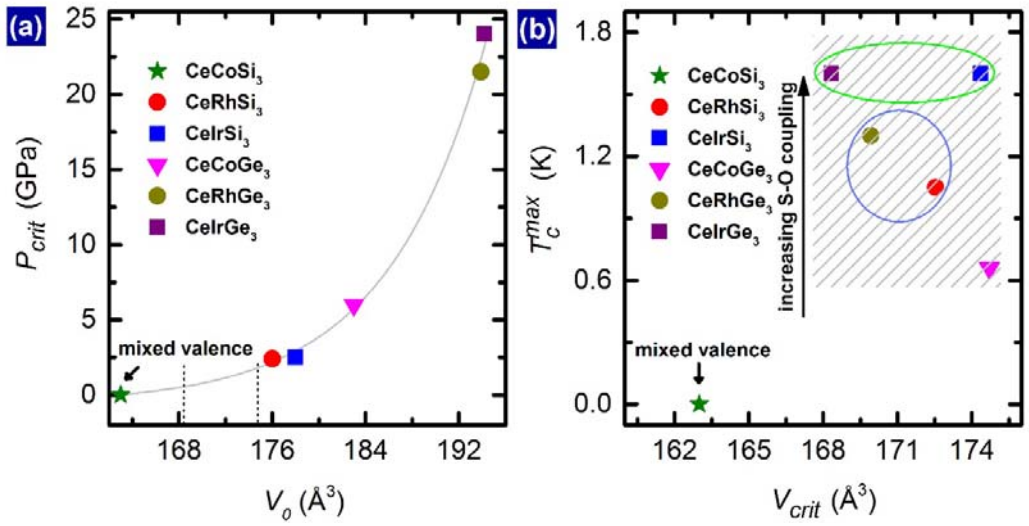

Figure 7 Correlations among $CeTX_3$ ambient-pressure cell volume, critical pressure P_{crit} for developing a maximum superconducting transition T_C^{max} and cell volume at T_C^{max}. (a) Critical pressure where T_C reaches its maximum value as a function of ambient-pressure unit cell volume V_0. The vertical dashed lines along the abscissa reflect the range of volumes marked by the hashed box in (b). (b) Plot of maximum T_C versus unit-cell volume V_{crit} where a maximum T_C is observed. The critical volume for superconducting $CeRhGe_3$ is determined from the equation of state (Fig. 5d): $V_{crit} = V_0 \times [1+P_{crit} \times (B'/B)]^{-1/B'}$ with B = 115 GPa and B' = 5. We assume this same relationship to estimate V_{crit} for other family members.